ELSEVIER

International Journal of Mass Spectrometry 179/180 (1998) 103–115

International Journal of Mass Spectrometry

Gas phase activation of carbon dioxide by niobium and niobium monoxide cations

M.R. Sievers, P.B. Armentrout*

Department of Chemistry, University of Utah, Salt Lake City, UT 84112, USA

Received 26 March 1998; accepted 1 June 1998

Abstract

Guided ion beam mass spectrometry is used to investigate the kinetic energy dependence of the reactions of Nb^+ (^5D) and NbO^+ ($^3\Sigma^-$) with CO_2, and the reverse pathways, NbO^+ ($^3\Sigma^-$) and NbO_2^+ with CO. These systems exhibit complicated behavior because the ground states of the reactants and products have different spins. To further probe the potential energy surfaces for these reaction systems, NbO_2^+ and the intermediates, $ONb(CO)^+$, $ONb(CO_2)^+$, and $O_2Nb(CO)^+$, are studied by collisional activation experiments with Xe. Analysis of the reaction cross sections obtained in this study yield (in eV) $D_0(Nb^+–CO) = 0.99 \pm 0.05$, $D_0(ONb^+–CO) = 1.10 \pm 0.05$, $D_0(ONb^+–CO_2) = 0.88 \pm 0.03$, $D_0(O_2Nb^+–CO) = 1.11 \pm 0.05$, and $D_0(ONb^+–O) = 5.71 \pm 0.17$. Speculative determinations of electronic excitation energies for two states each of NbO^+ and of NbO_2^+ are also made. Combining the results obtained from this study and those obtained from the literature, we are able to generate a fairly complete potential energy surface for the Nb^+ reaction system. We also compare the reactivities of Nb^+, NbO^+, and NbO_2^+ with respect to the interconversion of CO and CO_2. (Int J Mass Spectrom 179/180 (1998) 103–115)

Keywords: CO_2 activation; Bond energies; Niobium monoxide cations; Niobium dioxide cations; Guided ion beam mass spectrometry

1. Introduction

The use of metal and metal oxide catalysts to convert carbon dioxide and carbon monoxide to more useful chemical materials is an active field of study [1–12]. One benefit of such chemistry is the removal of one abundant constituent of greenhouse gases, carbon dioxide. Some fundamental insight into such processes can be achieved by studying the reactions of metal and metal oxide cations with CO or CO_2 in the gas phase using a guided ion beam mass spectrometer. Such work can elucidate the energetics of the reactions, their mechanisms, and details of the potential energy surfaces.

Previous gas phase studies of the interaction of metal cations with CO_2 and of metal oxide cations with CO were performed using ion cyclotron resonance (ICR) mass spectrometry. Kappes and Staley used ICR to study the oxidation reactions of bare metal cations with carbon dioxide [13,14]. In the case of Fe, they observed that FeO^+ (formed by the reaction of $Fe^+ + N_2O$) oxidizes CO to CO_2 at thermal energies. Kikthenko et al. used ICR to study the reactions of Mo^+ and W^+ in mixtures of CO and

* Corresponding author.

Dedicated to Professor Fulvio Cacace for his many contributions to ion chemistry.

1387-3806/98/$19.00
PII S1387-3806(98)14064-2

N_2O [15]. They observed indirect evidence for the oxidation of CO to CO_2 by MoO_3^+ and WO_3^+. Matsuda and co-workers have studied reactions of mixtures of metal carbonyls, $Cr(CO)_6$ [16], $Fe(CO)_5$ [17], and $Ni(CO)_4$ [18] with CO and O_2 initiated by shock waves. Kinetic analysis of their data is used to infer oxidation of CO by CrO_m (m = 1, 2, 3), Fe_nO_m, and NiO. Wesendrup and Schwarz used ICR to study the reactions of $Ta(O)CH_2^+$ with CO_2 and found that ketene could be formed [19]. Previously, we used guided ion beam mass spectrometry to examine the $V^+ + CO_2 \rightarrow VO^+ + CO$ reaction system in detail [20]. This reaction exhibited a cross section with a very complicated energy dependence. Analysis of this cross section resulted in the accurate determination of excitation energies for VO^+ as confirmed by a photoelectron study of VO by Dyke et al. [21]. The present work extends these studies to niobium, the second row congener of vanadium.

A very important consideration in the systems studied here is the electronic state of the metal, metal monoxide, and metal dioxide cations. The ground state of Nb^+ is $^5D(4d^4)$ with low lying excited states (in eV) at 0.29 (^5F, $5s^14d^3$), 0.69 (^3P, $4d^4$), 0.93 (^3F, $5s^14d^3$), 1.18 (^3H, $4d^4$), and 1.27 (^3G, $4d^5$) above the ground state [22]. The electronic states of NbO^+ come from a photoelectron study by Dyke et al. [23]. They measured the vertical ionization energies (IEs) of the ground state and low lying excited states of NbO^+ from ground state NbO ($^4\Sigma^-$). The ground state of NbO^+ is $^3\Sigma^-(2\sigma^21\pi^41\delta^2)$ with a vertical IE of 7.91 ± 0.02 eV. They determined the first excited state ($^3\Delta$, $2\sigma^23\pi^41\delta^13\sigma^1$) to have a vertical IE of 10.34 ± 0.02 eV, an excitation energy of 2.43 ± 0.03 eV above the ground state. They were also able to measure vertical IEs for two higher excited states that correspond to removal of a bonding π electron, 11.43 ± 0.04 eV, or bonding σ electron, 12.64 ± 0.04 eV. The vertical IEs correspond to $^5\Pi$ and $^5\Sigma^-$ states lying 3.52 ± 0.04 and 4.73 ± 0.04 eV above the ground state, respectively. The ground state for the metal dioxide is unknown theoretically or experimentally, but theoretical calculations [24] on the isovalent ZrO_2 neutral molecule find it to have a $^1A_1$ ground state. Therefore it seems reasonable to believe that NbO_2^+ also has a singlet ground state. We also presume that the geometry of NbO_2^+ is bent, as found for ZrO_2 in the theoretical study. A bent geometry allows all of the Nb^+ and Zr orbitals to contribute to bonding the O atoms. Overall, these considerations show that the reactions of ground state $Nb^+(^5D)$ and $NbO^+(^3\Sigma^-) + CO_2(^1\Sigma_g^+)$ cannot form ground state $NbO^+(^3\Sigma^-)$ and $NbO_2^+(^1A_1) + CO(^1\Sigma^+)$ products, respectively, in spin-allowed processes.

2. Experimental

2.1. General

These studies are performed by using a guided ion beam tandem mass spectrometer. The instrument and experimental methods have been described previously [25,26]. Ions, formed as described below, are extracted from the source, accelerated, and focused into a magnetic sector momentum analyzer for mass analysis. The ions are decelerated to a desired kinetic energy and focused into an octopole ion guide that radially traps the ions. While in the octopole, the ions pass through a gas cell that contains the neutral reactant at pressures where multiple collisions are improbable (<0.30 mTorr). Single collision conditions were verified by examining the pressure dependence of the cross sections measured here. The product ions and the reactant ion beam drift out of the gas cell, are focused into a quadrupole mass filter and then detected by a secondary electron scintillation detector. Ion intensities are converted to absolute cross sections as described previously [25]. Uncertainties in the absolute cross sections are estimated at ±20%.

To determine the absolute zero and distribution of the ion kinetic energy, the octopole is used as a retarding energy analyzer [25]. The uncertainty in the absolute energy scale is ±0.05 eV (lab). The full width at half maximum (fwhm) of the ion energy distribution is 0.2–0.4 eV (lab). Lab energies are converted into center-of-mass energies by using

$E(\mathrm{CM}) = E(\mathrm{lab})m/(m + M)$ where M and m are the masses of the ion and neutral reactant, respectively. All energies stated in this article are in the center-of-mass frame, unless noted otherwise.

2.2. Ion source

The ion source used here is a dc discharge/flow tube (DC/FT) source described in previous work [26]. The DC/FT source utilizes a niobium cathode held at 1.5–3 kV over which a flow of approximately 90% He and 10% Ar passes at a typical pressure of ~0.5 Torr. Ar^+ ions created in a direct current discharge are accelerated toward the niobium cathode, sputtering off atomic metal ions. The ions then undergo ~10^5 collisions with He and ~10^4 collisions with Ar in the meter long flow tube before entering the guided ion beam apparatus. From results obtained previously [27], we believe that the ions produced in the DC/FT source are exclusively in their a^5D ground state, and we assume the populations of the spin-orbit levels have a Maxwell-Boltzmann distribution at 300 ± 100 K.

Ground state NbO^+ and NbO_2^+ were made by allowing Nb^+ (created in the dc discharge) to react with O_2 introduced ~25 cm downstream into the flow tube at ~2 m Torr. $ONb^+(CO)$ and $O_2Nb(CO)^+$ were produced by allowing the Nb^+ to react with O_2 upstream in the flow tube and CO downstream. $ONb^+(CO_2)$ was produced by allowing the NbO^+ to interact with CO_2 downstream in the flow tube. Three-body collisions with the He/Ar flow gas stabilize these species and the large number of collisions between the ions and the bath gases should thermalize the ions both rotationally and vibrationally. We assume that these ions are in their ground electronic states and that the internal energy of these clusters is well described by a Maxwell-Boltzmann distribution of rotational and vibrational states corresponding to 300 ± 100 K. Previous work from this laboratory, including studies of N_4^+ [28], $Fe(CO)_x^+$ (x = 1–5) [29], $Cr(CO)_x^+$ (x = 1–6) [30], and $H_3O^+(H_2O)_x$ (x = 1–5) [31] have shown that these assumptions are usually valid.

Attempts were also made to produce $Nb^+(CO_2)$. Addition of CO_2 downstream in the flow tube did produce a cation that had a mass of $Nb^+(CO_2)$, but collision-induced dissociation (CID) experiments performed on this cation yielded results consistent with a $ONb^+(CO)$ structure rather than the CO_2 ligated niobium cation. In addition, ligand exchange reactions between $Nb^+(N_2)$ and CO_2 in the flow tube did not form any ions that could be identified as having the $Nb^+(CO_2)$ structure.

2.3. Data analysis

Previous theoretical [32,33] and experimental work [34] has shown that endothermic cross sections can be modeled by using Eq. (1),

$$\sigma(E) = \sigma_0 \Sigma\, g_i(E + E_{\mathrm{rot}} + E_i - E_0)^n/E \qquad (1)$$

where σ_0 is an energy independent scaling parameter, E is the relative translational energy of the reactants, E_{rot} is the average rotational energy of the reactants, E_0 is the reaction threshold at 0 K, and n is an energy independent scaling parameter. The summation is over each vibrational state of the reactants having relative populations g_i and energies E_i. The various sets of vibrational frequencies used in this work are listed in Table 1. The vibrational frequency for NbO^+ was taken from the study of Dyke et al. [23]. Frequencies for NbO_2^+ were taken from electron diffraction work on NbO_2 [35]. The frequencies for CO and CO_2 were taken from the literature [36,37]. The vibrational frequencies for $ONb^+(CO)$, $O_2Nb^+(CO)$, and $ONb^+(CO_2)$ were taken to equal the vibrational frequencies of NbO^+ or NbO_2^+, and CO or CO_2 plus sets of frequencies for the metal oxide-ligand modes that are similar to those we have used previously for $CrCO^+$, for the carbonyl systems, and $V^+(CO_2)$, for the CO_2 system [20,30]. The frequencies used in this study are estimates and therefore were varied by ±20% in the data analysis.

Before comparison with the data, the model is convoluted over the neutral and ion kinetic energy distributions using previously developed methods [25]. The parameters E_0, σ_0, and n are then optimized

Table 1
Molecular vibrational frequencies

Species		Frequencies, (cm^{-1})[a]
NbO^+[b]		1067
NbO_2^+[c]		527, 854, 1009
CO_2[d]		667(2), 1333, 2349
CO[e]		2214.2
$ONb^+(CO)$	(1)[f]	35(2), 166, 221(2) + $\nu(NbO^+)$ + $\nu(CO)$
	(2)[f]	20(2), 100, 150(2) + $\nu(NbO^+)$ + $\nu(CO)$
$ONb^+(CO_2)$	(1)[f]	150(2), 200(2) + $\nu(NbO^+)$ + $\nu(CO_2)$
	(2)[g]	25, 105, 196, 200, 600, 935, 1067, 1176, 1745
$O_2Nb^+(CO)$	(1)[f]	20(2), 100, 150(2) + $\nu(NbO_2^+)$ + $\nu(CO)$
	(2)[f]	35(2), 166, 221(2) + $\nu(NbO_2^+)$ + $\nu(CO)$

[a] Numbers in parentheses denote the degeneracy of the vibration.
[b] Estimated as equal to those for neutral NbO_2 from [23].
[c] [35].
[d] [36].
[e] [37].
[f] Estimates. See text for details.
[g] $V^+(CO_2)$ frequencies from [20] and estimates for two bends (25 and 200 cm^{-1}).

using a nonlinear least squares analysis in order to best reproduce the data. Reported values of E_0, σ_0, and n are mean values for each parameter from the best fits to several independent sets of data and uncertainties are one standard deviation from the mean. The listed uncertainties in the E_0 values also include the uncertainty in the absolute energy scale and uncertainties introduced by the estimated vibrational frequencies used for the various complexes studied.

3. Results

3.1. $Nb^+ + CO_2$

Niobium cations react with carbon dioxide to form three products in reactions (2)–(4), as shown in Fig. 1:

$$Nb^+ + CO_2 \rightarrow NbO^+ + CO \quad (2)$$

$$\rightarrow NbCO^+ + O \quad (3)$$

$$\rightarrow NbO_2^+ + C \quad (4)$$

Literature thermochemistry shown in Table 2 establishes that reaction (2) is exothermic by 1.68 ± 0.11 eV. The NbO^+ cross section does show exothermic

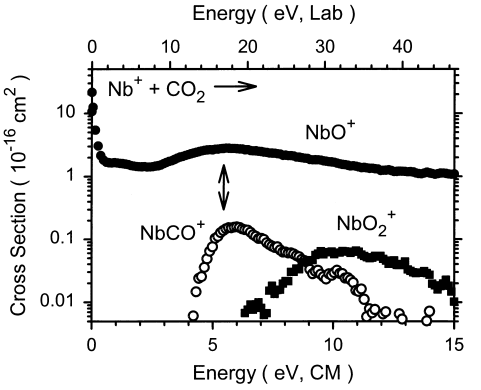

Fig. 1. Product cross sections for $Nb^+ + CO_2$ as a function of collision energy in the center of mass frame (lower x axis) and laboratory frame (upper x axis). The arrow marks the bond dissociation energy of CO_2 at 5.45 eV.

reaction behavior up to near 0.5 eV. The cross section then plateaus before rising again near 2.5 eV. Near 6 eV, the NbO^+ cross section reaches a maximum and begins to fall off. This decline is characteristic of the onset of reaction (5),

$$Nb^+ + CO_2 \rightarrow Nb^+ + O + CO \quad (5)$$

dissociation of NbO^+, which can begin at D_0(OC–O), Table 2.

Fig. 2 displays the threshold region for reaction (2). There are three features evident in the NbO^+ cross section. A model with an energy dependence of

Table 2
Bond dissociation energies at 0 K

Bond	Bond energy (eV)
C–O	11.108 ± 0.005[a]
OC–O	5.453 ± 0.002[a]
Nb^+–O	7.13 ± 0.11[b]
Nb^+–CO	0.82 ± 0.13[c], 0.99 ± 0.05[d]
ONb^+–O	5.71 ± 0.17[d]
ONb^+–CO	1.10 ± 0.05[d]
ONb^+–CO_2	0.88 ± 0.03[d]
O_2Nb^+–CO	1.11 ± 0.05[d]

[a] Calculated from data in S.G. Lias, J.E. Bartmess, J.F. Liebman, J.L. Holmes, R.D. Levin, W.G. Mallard, J. Phys. Chem. Ref. Data 17 (1988) Suppl. 1.
[b] M.R. Sievers, Y.-M. Chen, P.B. Armentrout, J. Chem. Phys. 105 (1996) 6322.
[c] [38].
[d] This work.

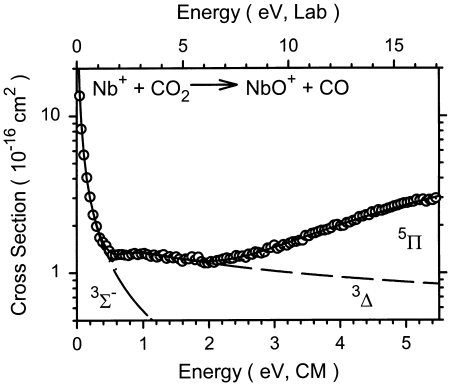

Fig. 2. Product cross section for $Nb^+ + CO_2$ to form $NbO^+ + CO$ in the threshold region as a function of collision energy in the center of mass frame (lower *x* axis) and laboratory frame (upper *x* axis). The dashed lines show models for formation of ground state $NbO^+(^3\Sigma^-)$ and the sum of this model and that for formation of $NbO^+(^3\Delta)$. The solid line running through the data points shows the sum of these two models and that for the formation of $NbO^+(^5\Pi)$ convoluted with the experimental energy distributions. The optimized parameters used in Eq. (1) for the latter two models are listed in Table 3.

$E^{-1.0\pm0.1}$ reproduces the data up to a kinetic energy of about 0.5 eV. Above this energy, the NbO^+ cross section can be reproduced by introducing two more models. The optimum parameters of Eq. (1) for these models are given in Table 3. Addition of these three models reproduces the NbO^+ cross section accurately up to 5 eV as shown in Fig. 2. The interpretation of this complex behavior is discussed below.

The formation of $NbCO^+$ begins near 4 eV. Analysis of this cross section (Table 3) yields a threshold of 4.46 ± 0.05 eV, which can be combined with D_0(OC–O) to yield $D_0(Nb^+–CO) = 0.99 \pm 0.05$ eV. This is in reasonable agreement with the theoretical value of 0.82 ± 0.13 eV calculated by Barnes et al. [38]. This cross section also reaches a maximum near D_0(OC–O), indicating that its decline is due to reaction (5), dissociation of the $NbCO^+$ product.

Formation of NbO_2^+ in reaction (4) is not observed until an apparent threshold near 6 eV. This cross section reaches a maximum near 10 eV, consistent with the dissociation of this ion to form $NbO^+ + O$, equivalent to reaction (6),

$$Nb^+ + CO_2 \rightarrow NbO^+ + O + C \quad (6)$$

beginning at 9.43 ± 0.11 eV. Dissociation to $Nb^+ + O_2 + C$, beginning at 11.4 eV is also plausible but CID studies of NbO_2^+ (see below) yield no observable Nb^+ product. The elevated thresholds and competition with the much more favorable reaction (2) explain the small size of the cross sections for reactions (3) and (4). Analysis of this slowly rising NbO_2^+ cross section results in a threshold of 5.1 ± 0.4 eV. This would correspond to $D_0(ONb^+–O) = 4.3 \pm 0.4$ eV if the threshold occurred promptly at the thermodynamic limit. Evidence against this is discussed below.

3.2. $NbO^+ + CO$

The reaction of NbO^+ and CO, shown in Fig. 3, forms two products in reactions (7)–(9).

$$NbO^+ + CO \rightarrow Nb^+ + O + CO \quad (7)$$

$$\rightarrow Nb^+ + CO_2 \quad (8)$$

Table 3
Optimized parameters of Eq. (1) for $Nb^+ + CO_2$ system

Reaction	σ_0	n	E_0, eV
$Nb^+ + CO_2 \rightarrow NbO^+ + CO$	1.34 (0.03)	0.7 (0.1)	0.58 (0.04)
	0.90 (0.34)	2.0 (0.3)	1.89 (0.18)
$\rightarrow NbCO^+ + O$	1.26 (0.11)	1.8 (0.2)	4.46 (0.05)
$\rightarrow NbO_2^+ + C$	0.02 (0.01)	2.5 (0.5)	5.1 (0.4)
$NbO^+ + CO \rightarrow Nb^+ + CO_2$	0.0017 (0.0003)	2.5 (0.2)	2.37 (0.11)[a]
$\rightarrow Nb^+ + O + CO$	0.18 (0.08)	2.0 (0.2)	7.7 (0.3)
$\rightarrow NbO_2^+ + C$	0.32 (0.11)	2.0 (0.2)	5.60 (0.20)
$ONb^+(CO) + Xe \rightarrow NbO^+ + CO + Xe$	15.1 (2.3)	1.4 (0.2)	1.10 (0.05)

[a] Calculated threshold for the formation of $Nb^+(^3P) + CO_2$. See text for details.

$$\rightarrow NbO_2^+ + C \quad (9)$$

The Nb^+ cross section slowly rises from an apparent threshold near 2–3 eV until near 7 eV, at which point it rises much more rapidly. The latter feature corresponds to reaction (7), simple CID, which can begin at $D_0(Nb^+–O)$, Table 2. Thus, the lower energy feature must be due to reaction (8), the reverse of reaction (2) and endothermic by 1.68 ± 0.11 eV. Near 5 eV, the NbO_2^+ cross section starts to rise. It continues to increase until near 11 eV, where it can dissociate to NbO^+ and O, starting at $D_0(CO)$. The measured threshold for reaction (9) of 5.60 ± 0.20 eV (Table 3) can be combined with $D_0(CO)$ to yield $D_0(ONb^+–O)$ = 5.51 ± 0.20 eV.

The observation of a higher apparent threshold than predicted for formation of Nb^+ and CO_2, reaction (8), is similar to our observations for reactions involving the first row congener, vanadium [20]. In that study, the reaction, $VO^+ + CO \rightarrow V^+ + CO_2$, was observed to proceed efficiently through a spin-conserved pathway to form an excited triplet state of the vanadium cation. No evidence for formation of the ground quintet state of V^+ was observed. Because both VO^+ and NbO^+ have triplet ground states and both V^+ and Nb^+ have quintet ground states, we postulate that the niobium system behaves similarly. Given the literature thermochemistry in Table 2, the calculated E_0 threshold values for formation of ground state CO_2 and Nb^+ in its low-lying electronic states are 1.68 eV for ^5D, 1.97 eV for ^5F, 2.37 eV for ^3P, 2.61 eV for ^3F, and 2.86 eV for ^3H. The NbO^+ cross section can be modeled most easily with thresholds consistent with the formation of the ^3P or ^3F states of Nb^+ combined with a model for simple CID of NbO^+ with CO. This is shown in Fig. 3. Use of the other Nb^+ thresholds led to models that are considerably worse reproductions of the data, however, the noise level of the Nb^+ cross section does not allow a definitive assessment of which electronic state, triplet or quintet spin, corresponds to the lower energy rise of the data. The ^3P state is a reasonable candidate and parallels our conclusions for the vanadium system [20].

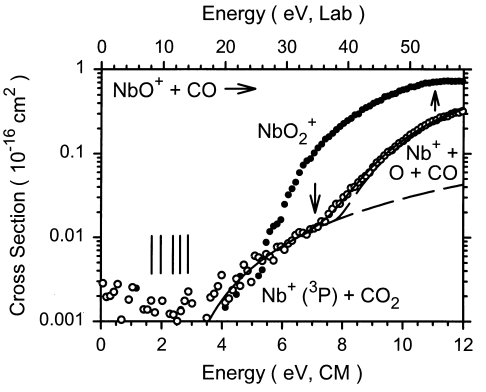

Fig. 3. Product cross sections for $NbO^+ + CO$ as a function of collision energy in the center of mass frame (lower *x* axis) and laboratory frame (upper *x* axis). Arrows mark the bond dissociation energies of NbO^+ at 7.13 eV and CO at 11.11 eV. The dashed lines are the model of Eq. (1) with the optimized parameters listed in Table 3 for the formation of $Nb^+(^3P) + CO_2$ and for simple CID to $Nb^+ + O + CO$. The solid line shows the sum of the two models convoluted over the experimental energy distributions. Vertical lines indicate the thresholds for the ^5D, ^5F, ^3P, ^3F, and ^3H states of Nb^+ at 1.68, 1.97, 2.37, 2.61, and 2.86 eV, respectively.

3.3. $ONb^+(CO) + Xe$

Collisional activation of $ONb^+(CO)$ with Xe yields the formation of only one product, NbO^+, in reaction (10), as shown in Fig. 4.

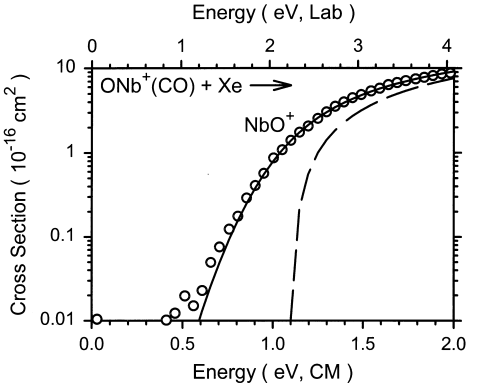

Fig. 4. Product cross sections for $ONb^+(CO) + Xe$ as a function of collision energy in the center of mass frame (lower *x* axis) and laboratory frame (upper *x* axis). The dashed line is the model of Eq. (1) with the optimized parameters listed in Table 3 for the CID process. The solid line shows this model convoluted with the experimental energy distributions.

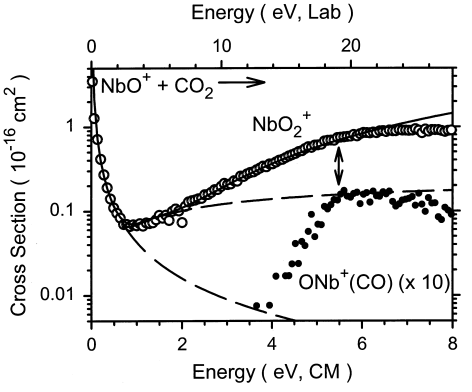

Fig. 5. Product cross sections for $NbO^+ + CO_2$ as a function of collision energy in the center of mass frame (lower *x* axis) and laboratory frame (upper *x* axis). The arrow marks the bond dissociation energy of CO_2 at 5.45 eV. The dashed lines show the three models needed to reproduce the NbO_2^+ cross section (see text) and the solid line is the sum of these models convoluted over the experimental energy distributions.

$$ONb^+(CO) + Xe \rightarrow NbO^+ + CO + Xe \quad (10)$$

The cross section rises from an apparent threshold near 0.5 eV and continues to increase until near 2 eV where it starts to level off. Analysis of this cross section with Eq. (1) yields the optimized parameters in Table 3. The threshold of 1.10 ± 0.05 eV is assigned to the ONb^+–CO bond dissociation energy.

3.4. $NbO^+ + CO_2$

Two products are observed in the reaction of NbO^+ with CO_2, as shown in Fig. 5. These can be formed in reactions (11) and (12).

$$NbO^+ + CO_2 \rightarrow NbO_2^+ + CO \quad (11)$$

$$\rightarrow NbCO_2^+ + O \quad (12)$$

The NbO_2^+ product cross section shows a feature that exhibits exothermic reaction behavior, which indicates that $D_0(ONb^+–O) > D_0(OC–O) = 5.45$ eV (Table 2). From 0 to near 1 eV, the reaction cross section decreases as $E^{-1.5\pm0.1}$. Near 1 eV, the NbO_2^+ cross section starts to slowly rise and continues rising until near 6 eV where it levels off. This is attributed to dissociation of the NbO_2^+ product which can begin at $D_0(CO_2)$ through reaction (13).

$$NbO^+ + CO_2 \rightarrow NbO^+ + O + CO \quad (13)$$

To reproduce the NbO_2^+ cross section up to near 6 eV, the exothermic decline must be combined with two more models with optimum parameters given in Table 4. The uncertainties in the thresholds include consideration of all reasonable models for the exothermic cross section at lower energy. The cross section could not be accurately reproduced if only one endothermic model were included. The sum of these three model cross sections accurately reproduces the NbO_2^+ cross section as shown in Fig. 5. The interpretation of this complex behavior is discussed below.

The $NbCO_2^+$ product cross section rises from an apparent threshold near 4 eV. The cross section rises to an energy consistent with the onset of reaction (13) and then declines slowly. It seems likely that this product has a ONb^+–CO structure as the cross section behaves similarly to that for reaction (3). Analysis of this reaction cross section gives a threshold of 4.45 ±

Table 4
Optimized parameters of Eq. (1) for $NbO^+ + CO_2$ system

Reaction	σ_0	n	E_0, eV
$NbO^+ + CO_2 \rightarrow NbO_2^+ + CO$	0.13 (0.01)	1.2 (0.2)	0.79 (0.11)
	0.11 (0.10)	2.5 (0.4)	1.70 (0.39)
$\rightarrow NbCO_2^+ + O$	0.06 (0.02)	1.5 (0.4)	4.45 (0.16)
$NbO_2^+ + CO \rightarrow NbO^+ + CO_2$	0.012 (0.004)	2.5 (0.2)	1.12 (0.17)
$\rightarrow NbO^+ + O + CO$	0.14 (0.05)	2.4 (0.2)	5.29 (0.21)
$ONb^+(CO_2) + Xe \rightarrow NbO^+ + CO_2 + Xe$	19.2 (0.4)	1.1 (0.1)	0.88 (0.03)
$\rightarrow NbO_2^+ + CO + Xe$	2.37 (0.13)	1.3 (0.3)	0.59 (0.07)
$O_2Nb^+(CO) + Xe \rightarrow NbO_2^+ + CO + Xe$	9.72 (1.0)	1.7 (0.2)	1.11 (0.05)
$NbO_2^+ + Xe \rightarrow NbO^+ + O + Xe$	0.35 (0.08)	1.9 (0.1)	5.87 (0.19)

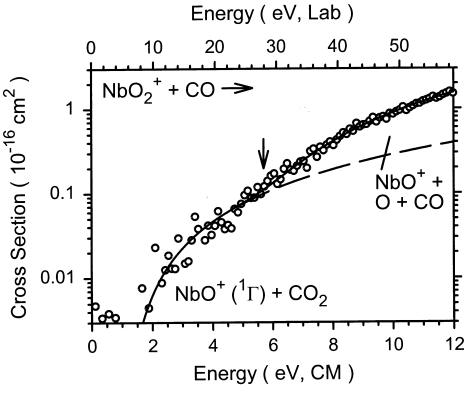

Fig. 6. Product cross section for NbO_2^+ + CO to form NbO^+ as a function of collision energy in the center of mass frame (lower *x* axis) and laboratory frame (upper *x* axis). The arrow marks the bond dissociation energy of ONb^+–O at 5.71 eV. The dashed line is the model of Eq. (1) with the optimized parameters listed in Table 4 for process (14). The solid line shows the sum of this model with one for CID, process (15), convoluted over the experimental energy distributions.

0.16 eV, corresponding to $D_0(ONb^+–CO) = 1.00 \pm 0.16$ eV. This is consistent with the directly measured bond energy of 1.10 ± 0.05 eV (Tables 2 and 3) confirming the structural hypothesis.

3.5. NbO_2^+ + CO

The reaction of NbO_2^+ with CO results in the formation of one product, shown in Fig. 6, that can be formed in reactions (14) and (15).

$$NbO_2^+ + CO \rightarrow NbO^+ + CO_2 \quad (14)$$

$$\rightarrow NbO^+ + O + CO \quad (15)$$

The NbO^+ cross section rises slowly from an apparent threshold of 1–2 eV until past 14 eV. Analysis of the low energy feature of the NbO^+ cross section gives a threshold of 1.12 ± 0.17 eV, but this model fails to reproduce the data past about 5 eV, as shown in Fig. 6. At higher energies, a model for CID of the metal dioxide cation, reaction (15), is needed. The sum of these two models (with parameters in Table 4) allows the data to be reproduced well until near 12 eV.

This behavior of the cross sections for reactions (14) and (15) is qualitatively similar to that for reactions (7) and (8), Fig. 3. As in the NbO^+ + CO system, it seems likely that process (14) will be most efficient if it is spin conserving, but this requires formation of the NbO^+ product in a singlet spin state. Calculated thresholds, in eV, for reformation of CO_2 and NbO^+ in its ground and known excited states are 0.26 ± 0.24 for $^3\Sigma^-$, 2.69 ± 0.24 for $^3\Delta$, 3.78 ± 0.24 for $^5\Pi$ and 4.99 ± 0.24 eV for $^5\Sigma^-$. Hence, the threshold measured here is 0.86 ± 0.17 eV above the formation of ground state $NbO^+(^3\Sigma^-)$ and lies well below the thresholds for the other known states of NbO^+. We anticipate that a singlet excited state of NbO^+ would correspond to singlet coupling two of the nonbonding electrons of ground state NbO^+, $^3\Sigma^-(2\sigma^2 1\pi^4 1\delta^2)$, which should form NbO^+ in either a $^1\Gamma$ or $^1\Sigma^+$ both having $(2\sigma^2 1\pi^4 1\delta^2)$ configurations. This state was not considered by Dyke et al. [23] because it is not accessible in a one-electron ionization process from $NbO(^4\Sigma^-)$. We now note that the 0.86 ± 0.17 eV excitation energy measured here is comparable to the excitation energy of $Nb^+(^3P)$, 0.69 eV. This seems reasonable because this excitation also corresponds to singlet coupling two of the 4*d* electrons in the $^5D(4d^4)$ ground state.

3.6. $ONb^+(CO_2)$ + Xe

Collision-induced dissociation of the $ONb^+(CO_2)$ complex ion with Xe results in two products, shown in Fig. 7, formed by reactions (16) and (17):

$$ONb^+(CO_2) + Xe \rightarrow NbO^+ + CO_2 + Xe \quad (16)$$

$$\rightarrow NbO_2^+ + CO + Xe \quad (17)$$

The fact that the loss of CO_2 is the most efficient dissociation pathway for this complex indicates that the structure for this molecule is NbO^+ ligated by CO_2 rather than a different isomer of $NbCO_3^+$, e.g. $O_2Nb^+(CO)$. The NbO^+ cross section rises from an apparent threshold near 0.4 eV and then continues increasing until near 1.5 eV at which point it levels off. The threshold for the CID pathway of 0.88 ± 0.03 eV (Table 4) is assumed to equal $D_0(ONb^+–CO_2)$.

The NbO_2^+ cross section also starts to rise near 0.4 eV and continues until near 1 eV where it plateaus.

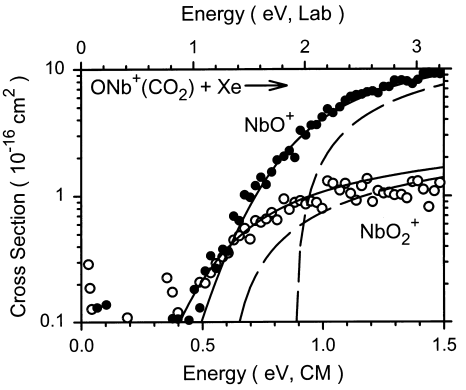

Fig. 7. Product cross sections for $ONb^+(CO_2)$ + Xe as a function of collision energy in the center of mass frame (lower *x* axis) and laboratory frame (upper *x* axis). The dashed lines are the models of Eq. (1) with the optimized parameters listed in Table 4 for processes (16) and (17). The solid lines show these models convoluted over the experimental energy distributions.

Analysis of this cross section yields a threshold 0.59 ± 0.07 eV (Table 4). This threshold can be combined with $D_0(ONb^+–CO_2)$ and $D_0(CO_2)$ to yield $D_0(ONb^+–O)$ = 5.74 ± 0.08 eV.

3.7. $O_2Nb^+(CO)$ + Xe

Collision-induced dissociation of the $O_2Nb^+(CO)$ complex yields one product in reaction (18). The cross section is qualitatively similar to that shown in Fig. 4:

$$O_2Nb^+(CO) + Xe \rightarrow NbO_2^+ + CO + Xe \qquad (18)$$

The observation that this product is the only observed decomposition pathway verifies the assignment of the structure of this molecule as NbO_2^+ ligated by CO. Further, if NbO_2^+ had a structure of molecular oxygen bound to Nb^+, i.e. $Nb^+(O_2)$, then we would anticipate seeing competitive loss of O_2. Failure to observe this process points to a niobium dioxo cation. This cross section rises rapidly from an apparent threshold near 0.6 eV. Analysis of the cross section for process (18) gives $D_0(O_2Nb^+–CO)$ = 1.11 ± 0.05 eV (Table 4). Unlike the dissociation behavior of the $ONb^+(CO_2)$ isomer, there is no observed formation of NbO^+ which is calculated to have a thermodynamic threshold of 1.35 ± 0.25 eV.

3.8. NbO_2^+ + Xe

Collision-induced dissociation of NbO_2^+ with Xe gives only one product in reaction (19).

$$NbO_2 + Xe \rightarrow NbO^+ + O + Xe \qquad (19)$$

The NbO^+ cross section rapidly rises from an apparent threshold near 5 eV. Analysis of the energy dependence of this cross section results in $D_0(ONb^+–O)$ = 5.87 ± 0.19 eV (Table 4). It is possible that this value is an upper limit because previous work done on the CID of diatomic metal oxide cations with Xe [39] has shown the thresholds measured are generally higher than bond energies measured using results from other reactions (e.g. M^+ + CO or $O_2 \rightarrow MO^+$ + C or O).

4. Discussion

4.1. NbO_2^+ thermochemistry

Thermochemical information about $D_0(ONb^+–O)$ can be obtained from reactions (4), (9), (11), (17), and (19). For the latter four reactions, the bond energies obtained compare reasonably well: 5.51 ± 0.20, >5.45, 5.74 ± 0.08, and 5.87 ± 0.19 eV, respectively. For reaction (4), the modeling of the true thermodynamic threshold is complicated because of competition with the more favorable production of NbO^+. Also, this reaction is spin forbidden which may grossly affect the threshold obtained (e.g. excited product states could be formed preferentially). Hence, the bond energy of 4.3 ± 0.4 eV is too low. We believe the best value for $D_0(ONb^+–O)$ obtained in this study is the average of the bond energies measured for reactions (9), (17), and (19), 5.71 ± 0.17 eV.

4.2. $NbCO_2^+$ potential energy surface

To understand these experiments in detail, we take the point of view that the experiments performed in this study ($Nb^+ + CO_2$, $NbO^+ + CO$, and ONb^+–CO CID) probe three separate places on the same set of potential energy surfaces for the $NbCO_2^+$ system. The

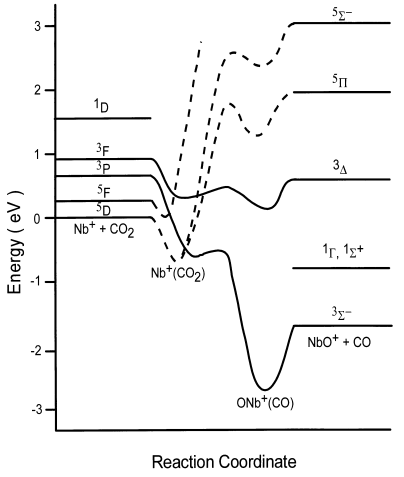

Fig. 8. The potential energy surfaces for the interaction of Nb^+ with CO_2 deduced in the present study. Solid lines show triplet surfaces while dashed lines indicate quintet surfaces. Energies of the asymptotes and the $ONb^+(CO)$ ground state are shown quantitatively. All other features are estimated (see text).

electronic states for the $Nb^+ + CO_2$ and $NbO^+ + CO$ asymptotes, described in the introduction, are shown in Fig. 8. The measurement of $D_0(ONb^+–CO)$ determines the well depth of this intermediate for ground state species. The well depth for $Nb^+–CO_2$ could not be measured in this study, therefore, we estimate the well depth as being equivalent to that of $V^+–CO_2$, 0.75 ± 0.04 eV [20]. We anticipate the bonding of Nb^+ with CO_2 and NbO^+ with CO is dominated by donation of ligand electrons into an empty 5*s* orbital on the metal and backdonation of electron density from metal $4d\pi$ orbitals into empty π-symmetry orbitals of the ligand. Bonding is enhanced when the 5*s* orbital is empty and the $4d\pi$ orbitals are occupied. Using this argument, we anticipate that Nb^+ states where the 5*s* orbital is occupied (the ^5F and ^3F) and NbO^+ states where the 3σ orbital, which has a great deal of 5*s* character, is occupied ($^3\Delta$, $^5\Pi$, and $^5\Sigma^-$) will have smaller bond energies. For Nb^+, the ^3P ($4d^4$) state binds more strongly to CO_2 than the ^5D ($4d^4$) state because two electrons, instead of one, can be used for π backbonding [40] into a single orbital on the ligand.

The asymptotes of $Nb^+ + CO_2$ and $NbO^+ + CO$ must now be connected. We expect that $Nb^+(^3P, 4d^4)$ will have a stronger interaction with CO_2 than $Nb^+(^3F,5s^14d^3)$, as noted above; therefore the lowest energy triplet state of $Nb^+(CO_2)$ correlates diabatically with $Nb^+(^3P)$. The lowest energy triplet state of $Nb^+(CO_2)$ is then taken to evolve to ground state $ONb^+(CO)$ and then to ground state $NbO^+(^3\Sigma^-)$ + $CO(^1\Sigma^+)$. The $NbO^+(^3\Delta)$ + $CO(^1\Sigma^+)$ product asymptote must adiabatically correlate with $Nb^+(^3F)$ + $CO_2(^1\Sigma_g^+)$ reactants in order to conserve electronic orbital angular momentum. The quintet surfaces can be created by connecting the quintet asymptotes of $Nb^+ + CO_2$ with the quintet states of $NbO^+ + CO$. The a^5D state of Nb^+ was directly correlated to both the $^5\Pi$ and $^5\Sigma^-$ states of NbO^+.

With these potential energy surfaces, we can now understand most of our experimental observations. At the lowest energies, $Nb^+(^5D)$ reacts with CO_2 to form $NbO^+(^3\Sigma^-)$ + $CO(^1\Sigma^+)$ in an exothermic reaction. The observation that there is no barrier to the reaction indicates that the transition state between $Nb^+(CO_2)$ and $ONb^+(CO)$ and the quintet-triplet surface crossing must have energies below the $Nb^+(^5D)$ + $CO_2(^1\Sigma_g^+)$ asymptote (Fig. 8). As the kinetic energy is increased, $Nb^+(^5D)$ reacts to form $NbO^+ + CO$ more efficiently. Our measured threshold for this increase, 0.58 ± 0.04 eV, is lower than that expected for appearance of $NbO^+(^3\Delta)$ + $CO(^1\Sigma^+)$ at 0.75 ± 0.11 eV, however this value is based on a vertical IE reported by Dyke et al. [23]. Our 0.58 eV threshold corresponds to an IE for NbO of 10.17 ± 0.12 eV. Careful examination of the photoelectron spectrum of NbO [23] shows that this energy corresponds to the initial onset of the ionization peak assigned to the $^3\Delta$ state of NbO^+. Thus we believe that the value determined here corresponds to the adiabatic IE for the $^3\Delta$ state of NbO^+.

At still higher kinetic energies, the cross section for $NbO^+ + CO$ increases again. This part of the cross section represents about 90% of the total cross section by about 6 eV (Fig. 2) showing that whatever process is leading to this feature is much more efficient than the processes leading to the lower energy features. This is consistent with formation of the quintet states of NbO^+ in a spin-allowed process. The threshold that we measure for this feature corresponds to an IE for

NbO of 11.48 ± 0.21 eV. This energy corresponds very nicely to the IE measured for the lowest energy quintet state of NbO^+ by Dyke et al. [23], IE($^5\Pi$) = 11.43 ± 0.04 eV.

When $NbO^+(^3\Sigma^-)$ reacts with CO ($^1\Sigma^+$), the dominant reaction is simple collision-induced dissociation, although inefficient production of $Nb^+ + CO_2$ is observed. Because this reverse reaction is likely to have a similar propensity for conserving spin as does the $Nb^+ + CO_2$ reaction, excited triplet states of Nb^+ should be the primary products in this reaction. This helps explain why the apparent threshold for formation of $Nb^+ + CO_2$ is higher than the thermodynamic threshold for forming $Nb^+(^5D)$, 1.68 ± 0.11 eV, but can be reproduced if the thresholds for production of the triplet states, $Nb^+(^3F)$ or $Nb^+(^3P) + CO_2(^1\Sigma_g^+)$, are used in Eq. (1). Presumably, reaction (8) is relatively inefficient because it is strongly endothermic and involves a complex rearrangement in order to break the strong Nb–O bond and form the O–CO bond.

When $ONb^+(CO)$ is collisionally activated, simple CID of the CO ligand dominates the product spectra (Fig. 4). This is clearly because ligand loss is much more facile and energetically favorable than the rearrangements necessary to form $Nb^+ + CO_2$. In addition, the potential energy surfaces in Fig. 8 show that this latter process does not conserve spin if ground state products are formed. If spin is conserved, formation of $Nb^+ + CO_2$ is even more endothermic, lowering its probability even further.

4.3. $NbCO_3^+$ system

Qualitatively, the $NbCO_3^+$ reaction system behaves similarly to the $NbCO_2^+$ system and we anticipate that the potential energy surfaces are comparable to those shown in Fig. 8. However, there is far less knowledge about the asymptotic energies of the $NbCO_3^+$ system compared to the $NbCO_2^+$ system, in particular with regard to the excitation energies of NbO_2^+. The thresholds determined here can be used to determine the energies of these product asymptotes assuming there are no barriers in excess of the endothermicity of the reaction process and the metal dioxide cation does not change its geometry (e.g. transforms from ONb^+–O to Nb^+–O_2). Such a transformation seems very unlikely given the very strong Nb^+–O and ONb^+–O bond energies (Table 2). Barriers cannot be discounted given the lack of detailed knowledge concerning the electronic structures of the ground and excited states of most species in this system, however, they seem no more likely than in the $NbCO_2^+$ system. Nevertheless, we can only speculatively assign our measured thresholds for reaction (11) to excitation energies for NbO_2^+ states of 1.05 ± 0.20 and 1.96 ± 0.43 eV. Given the parallels with the $NbCO_2^+$ system, it seems feasible that these correspond to an excited singlet state and an excited triplet state of NbO_2^+, respectively. We also note that the reverse reaction, process (14), appears to provide an estimate of the excitation energy of the lowest singlet state of NbO^+, 0.86 ± 0.24 eV for the $^1\Gamma$ or $^1\Sigma^+$ state, as shown in Fig. 8. This state appears not to be important in the $Nb^+ + CO_2 \rightarrow NbO^+ + CO$ system, which is reasonable because it involves yet another spin state.

4.4. Reactivity comparison

A strong influence on the metal oxide or dioxide cation's ability to convert CO_2 to CO and vice versa is the thermodynamics of the process. For CO_2 to CO conversion to be facile at thermal energies, the newly formed metal oxide bond must be greater than the 5.45 eV needed to break the C–O bond in CO_2. Both Nb^+–O and ONb^+–O satisfy this criterion (Table 2). Comparison of the NbO^+ and NbO_2^+ cross sections obtained from the reactions of Nb^+ and NbO^+ with CO_2, respectively (shown in Figs. 1 and 5) shows that Nb^+ is roughly five times more efficient than NbO^+ in converting CO_2 to CO in the energy range from 0–1 eV.

To convert CO to CO_2 at thermal energies, the oxidizer must have a bond energy lower than 5.45 eV. Neither NbO^+ nor NbO_2^+ fulfill this requirement such that these reactions are endothermic. To determine relative efficiencies for the NbO^+ and NbO_2^+ to convert CO to CO_2, we compare the Nb^+ and NbO^+ cross sections at low energies in Figs. 3 and 6, respectively. From this it appears that NbO_2^+ is nearly

10 times more efficient than NbO^+ in converting CO to CO_2, largely because of the much smaller endothermicity for the NbO_2^+ reaction.

5. Summary

We use guided ion beam mass spectrometry to study the kinetic energy dependences of the bimolecular reactions of Nb^+ and NbO^+ with CO_2 and NbO^+ and NbO_2^+ with CO and also the collisional activation of NbO_2^+, $ONb^+(CO)$, $ONb^+(CO_2)$, and $O_2Nb^+(CO)$ by Xe. Both the $NbCO_2^+$ and $NbCO_3^+$ reaction systems show a propensity for spin-conserving processes, although spin-forbidden reactions are observed. Analysis of the kinetic energy dependence of the cross sections allows thermochemistry of the collisionally activated species to be obtained. In addition, we are able to speculatively assign adiabatic excitation energies for the $^3\Delta$ and $^1\Gamma$ or $^1\Sigma^+$ excited states of NbO^+ and two excitation energies for NbO_2^+. Combined with literature information, the thermochemistry and reaction dynamics observed here allow us to construct a fairly complete potential energy surface for the interaction of Nb^+ with CO_2.

Acknowledgement

This research is supported by the National Science Foundation, grant no. CHE-9530412.

References

[1] W.M. Ayers (Ed.), Catalytic Activation of Carbon Dioxide, Proceedings of the ACS Symposium, Ser. 363, Washington, DC, 1988.
[2] A. Behr, Carbon Dioxide Activation by Metal Complexes, VCH, Weinheim, 1989.
[3] Y. Avila, J. Barrault, S. Pronier, C. Kappenstein, Appl. Catal. A. 132 (1995) 97.
[4] J. Miciukiewicz, T. Mang, Appl. Catal. A. 122 (1995) 151.
[5] T. Fujita, Y. Nishiyama, Y. Ohtsuka, K. Asami, K.-I. Kusakabe, Appl. Catal. A. 126 (1995) 245.
[6] T. Weimer, K. Schaber, M. Specht, A. Bandi, Energy Convers. Management 37 (1996) 1351.
[7] Y. Yanagisawa, Energy Convers. Management 36 (1995) 443.
[8] S.-E. Park, S.S. Nam, M.J. Choi, K.W. Lee, Energy Convers. Management 36 (1995) 573.
[9] M. Saito, T. Fujitani, I. Takahara, T. Watanabe, M. Takeuchi, Y. Kanai, K. Moriya, T. Kakumoto, Energy Convers. Management 36 (1995) 577.
[10] M. Hirano, T. Akano, T. Imai, K. Kuroda, Energy Convers. Management 36 (1995) 585.
[11] D.K. Otorbaev, Chem. Phys. 196 (1995) 543.
[12] M. Sahibzada, D. Chadwick, I.S. Metcalfe, Catal. Today 29 (1996) 367.
[13] M.M. Kappes, R.H. Staley, J. Phys. Chem. 85 (1981) 942.
[14] M.M. Kappes, R.H. Staley, J. Amer. Chem. Soc. 103 (1981) 1286.
[15] A.V. Kikthenko, V.B. Goncharov, K.I. Zamaraev, Catal. Lett. 21 (1993) 353.
[16] T.P.J. Izod, G.B. Kistiakowsky, S. Matsuda, J. Chem. Phys. 76 (1972) 2833.
[17] S. Matsuda, J. Chem. Phys. 57 (1972) 807.
[18] S. Matsuda, J. Phys. Chem. 76 (1972) 2833.
[19] R. Wesendrup, H. Schwarz, Angew. Chem. Int. Ed. Engl. 34 (1995) 2033.
[20] M.R. Sievers, P.B. Armentrout, J. Chem. Phys. 102 (1995) 754.
[21] J.M. Dyke, W.J. Gravenor, M.P. Hastings, A. Morris, J. Phys. Chem. 89 (1985) 4613.
[22] C.E. Moore, Atomic Energy Levels US GPO Circular No. 467, Washington, DC, 1952.
[23] J.M. Dyke, A.M. Ellis, M. Fehér, A. Morris, A.J. Paul, J.C.H. Stevens, J. Chem. Soc. Fara. Trans. 283 (1987) 1555.
[24] P.E.M. Siegbahn, J. Phys. Chem. 97 (1993) 9096.
[25] K.M. Ervin, P.B. Armentrout, J. Chem. Phys. 83 (1985) 166.
[26] R.H. Schultz, P.B. Armentrout, Int. J. Mass Spectrom. Ion Processes 107 (1991) 29.
[27] M.R. Sievers, Y.-M. Chen, J.L. Elkind, P.B. Armentrout, J. Phys. Chem. 100 (1996) 54.
[28] R.H. Schultz, P.B. Armentrout, J. Chem. Phys. 96 (1992) 1046.
[29] R.H. Schultz, K.C. Crellin, P.B. Armentrout, J. Am. Chem. Soc. 113 (1992) 8590.
[30] F.A. Khan, D.E. Clemmer, R.H. Schultz, P.B. Armentrout, J. Phys. Chem. 97 (1993) 7978.
[31] N.F. Dalleska, K. Honma, P.B. Armentrout, J. Am. Chem. Soc. 115 (1993) 12125.
[32] N. Aristov, P.B. Armentrout, J. Am. Chem. Soc. 108 (1986) 1806, and references therein.
[33] W.J. Chesnavich, M.T. Bowers, J. Phys. Chem. 83 (1979) 900.
[34] P.B. Armentrout, in Advances in Gas Phase Ion Chemistry, N.G. Adams, L.M. Babcock (Eds.), JAI, Greenwich, 1992, Vol. 1, pp. 83–119.
[35] A.G. Gershikov, V.P. Spiridinov, A. Ya. Prikhod'ko, E.V. Erokhin, High Temp. Sci. 14 (1981) 17.
[36] T. Shimanouchi, Table of Molecular Vibrational Frequencies, Consolidated, Vol. I, National Bureau of Standards, Washington, DC, 1972, p. 1.
[37] K.P. Huber, G. Herzberg, Molecular Spectra and Molecular Structure IV. Constants of Diatomic Molecules, Van Nostrand Reinhold Company, New York, 1979, Vol. IV, p. 1.

[38] L. A. Barnes, M. Rosi, C. W. Bauschlicher Jr., J. Chem. Phys. 93 (1990) 609.
[39] M.R. Sievers, Y.-M. Chen, P.B. Armentrout, J. Chem. Phys. 105 (1996) 6322.
[40] A. Dedieu, C. Bo, F. Ingold, in Metal-Ligand Interactions: From Atoms, to Clusters, to Surfaces, D.R. Salahub and N. Russo (Eds.), NATO Advanced Study Institute, Series C, Kluwer, Dordrecht, 1992, Vol. 378, p. 175.